Effect of thickness and annealing on mobility and crystallinity of CZTS films

S. RAQEEB, Y. KARAKUS*
Sakarya University, Science Faculty, Physics Department, Serdivan, Sakarya, Turkey

In this work CZTS thin films with different layers were coated on n-type Si substrate kept at 350 °C using the spray pyrolysis technique. FESEM results showed a crack-free and smooth surface. XRD results proved that all samples had a polycrystalline tetragonal type kesterite phase. Raman spectrum of the samples also confirmed the kesterite structures. The electrical measurements showed that all CZTS films had a p-type character with high absorption coefficient of 10^5 cm^{-1} and ideal band gap energy (1.52 eV). The effect of film thickness and annealing on the mobility of charged particles and the crystallinity was studied. An increase of more than one order of magnitude was observed in the mobility after increasing the thickness of the film. As the thickness increased from 0.15 μm to 11.6 μm, the mobility increased from 1.33 $cm^2V^{-1}S^{-1}$ to 30.5 $cm^2V^{-1}S^{-1}$. A significant enhancement was observed in XRD peaks through annealing. An increase of 30% was obtained in the XRD peak even at 150 °C. To our knowledge, this is the first time the effect of annealing at such low temperatures has been reported.

(Received May 31, 2023; accepted December 4, 2023)

Keywords: Spray pyrolysis, Annealing, XRD, Raman, UV-vis spectrum

1. Introduction

The use of coal, oil and natural gas for energy production has caused serious environmental problems such as global warming mainly due to carbon emission. Producing clean energy by the use of sustainable and renewable sources is of vital importance for solving all these environmental problems and also to meet the growing energy needs. Among the renewable energy sources the most abundant, sustainable and cheapest one is solar power. In spite of this abundancy, only 0.04% of basic power comes directly from solar sources [1]. Research done in the past two decades has concentrated mainly on finding highly efficient, stable, environmentally friendly and cheap photo-voltaic (PV) materials. These materials should also be highly absorptive, non-toxic and suitable for mass production.

The first generation PV materials consists of either single or poly silicon crystals [2-5]. The silicon solar cells are stable, have a high photo-voltaic conversion efficiency (PCE) (%26.7) [6], and are easy to produce on a large scale. The disadvantages of Si solar cells are the high cost and pollution caused by the Si raw material.

The second generation materials consists of semiconductors such as $Cu(In,Ga)(S,Se)_2$ (CIGS) and CdTe [7-9]. CIGS materials have a high PCE (23.35%) [10] and stability. The drawbacks of these materials are their high cost, scarcity of the Ga and In used in CIGS [11], and toxicity of the Cd in CdTe [11].

Third generation solar cells can be classified into three groups. The first two groups are organic material-based solar cells such as dye-sensitized solar cells (DSSCs) [12-14] and perovskites [15-19]. Although the efficiency of perovskite has increased immensely from 3.4% (2009) up to 28.3% (2021), perovskite suffers from a serious stability issue [19, 20]. The third group is the quaternary chalcogenide family Cu_2XSnS_4 (X = Ni, Zn, Co, Mn, Fe), namely Cu_2ZnSnS_4 (CZTS) [20-22].

Although the PCE of CZTS (12.6%) [23] is low compared to that of the previous two groups, it became an optimal material because of its ease of fabrication and low cost, high absorption coefficient (10^4 cm^{-1}), earth-abundance, ideal band gap (1.4 eV), and p-type conductivity [24-27].

Some of the reports published in the last decade are related to the effect of stoichiometry on the structural, optical and thermo-electrical properties of CZTS thin films [25, 28-30]. It has been reported that a Cu-poor, Zn-rich chemical composition causes a high carrier concentration [29, 30]. A Cu-rich, Zn-poor chemical composition causes an increase in crystallinity and band gap energy [31].

In other works, the effect of incorporating metal nanoparticles into CZTS has been investigated [32, 33]. It was reported that doping Ag nanoparticles into CZTS increased the electrical and decreased the thermal conductivity [32]. The doping of Na nanoparticles had similar effects on electrical and thermal conductivity [33]. While the measured conductivity of the bare CZTS sample was 852 Sm^{-1}; the conductivity of 0.5 wt% and 1 wt% Ag-doped samples were 4291 Sm^{-1} and 6369 Sm^{-1} respectively [32]. This enhancement in conductivity increased the figure of merit by 40% [33]. Additionally, an increase of more than 40% in PCE has been reported on Na-doped CZTS [34].

The effect of sulfurization on the thermal, optical, and electrical characteristics of CZTS thin films was also investigated [34]. Increasing the sulfurization duration has

caused an increase in the crystalline size of grown CZTS grains and the intensity of CZTS active modes, and has decreased the number of secondary modes [34].

Thermal annealing is an important step during manufacturing, which significantly affects morphology, improves the interface properties of the material, and eliminates the recombination centers at the p–n junction interface [20, 35–37]. Annealing has a considerable effect on the performance of all types of materials: polycrystalline (pc) Si-based [38], $Cu(In,Ga)(S,Se)_2$ [39], CdTe/CdS [40] and even polymer-based organic solar cell materials [41]. Because of stress and dislocations among the grain boundaries, the efficiency of pc-Si solar cells is less than that of the monocrystalline ones [42]. It is reported that annealing reduces the stress and dislocations, and increases the efficiency of pc-Si [38].

Various methods have been applied to CZTS thin film fabrication such as evaporation [43, 44], pulsed laser deposition [45], sputtering [46,47], spray pyrolysis [24, 25, 48], spin coating [49] etc. Each method has its own advantages and disadvantages. In this work the spray pyrolysis method was used because of its simplicity, moderate temperature processing, and ability to prepare homogeneous and highly crystalline thin films. Because of its decent characteristics such as excellent stability, earth-abundance, low cost, non-toxicity, high absorption and ideal band-gap energy, CZTS has been used as an absorber layer for solar cell applications.

In this paper, the morphological, structural, optical, and electrical characteristics of CZTS films have been analysed through FESEM, XRD, Raman spectroscopy, UV-Vis spectrophotometer and Hall-effect respectively. The effects of film thickness and annealing on mobility of charged particles and crystallinity of CZTS films were investigated.

2. Sample preparation

The precursor solution was prepared with 0.2M copper chloride (>99%, Sigma Aldrich), 0.1M zinc chloride (>99%, Sigma Aldrich), 0.1M tin chloride (>99%, Sigma Aldrich) and 1M thiourea (ACS reagent, ≥99.0%, Sigma Aldrich), which were dissolved separately in distilled water and mixed together before spraying. The solvent was a 60 ml mixture of ethanol in water: ethanol (20 ml), H_2O (40 ml). The final solution was filtered through a 2 μm pore-size PTFE filter. The substrate temperature was kept at 350 °C and the spray pyrolysis nozzle rate was 2 ml per minute. The substrate distance was 25 cm. Si substrates were etched within ethanol+HF (Hydrofluoric acid) for 10 min. Right after etching, Cu_2ZnSnS_4 layers were deposited onto the n-type Si substrate.

The crystal structures were determined using a Rigaku D/max-2400 Advanced XRD diffractometer. X-ray diffraction analysis was carried out at a speed of 1°/min in the 2θ range of 10-90° with CuK_α (λ= 1.5406 $\dot{A}$).

Surface morphology was studied with a FEI Quanta FEG450 FESEM. The Raman mapping of the CZTS thin films was done with a Raman RXN1, MR Probe. A λ= 785 nm diode laser was used as a light source. Raman spectra of the samples were taken in the 150-500 cm^{-1} spectral range. The film thickness was measured with SEM and FESEM.

3. Results and discussion

The FESEM images of the CZTS thin films are shown in Fig. 1. The nanoparticles forming the homogenous crystalline structure of CZTS were stuck together on the substrate which were kept at 350 °C. Morphology of the as-prepared Cu_2ZnSnS_4 layers showed a crack-free, smooth surface. The FESEM of the cross-section of four CZTS films are also shown in Fig.1. CZTS thin films at various thicknesses were fabricated at the range of 0.15-11.6 μm. Measured thickness of four different samples are given Fig.1 a)-d).

One can see from Fig.1 that as the thickness of a sample increases, the surface quality and crystallinity increase as well.

Optical properties of CZTS thin films were investigated through UV-vis absorption spectrum. One can see from Fig. 2 (a) that the absorption coefficient of CZTS samples is quite high in the entire visible range (10^5 cm^{-1}). Because of the higher thickness, we obtained an absorption coefficient one order of magnitude higher than the absorption values reported by various groups [16,24,26-33].

The band-gap of the CZTS were determined using an $(h\nu)^2$ vs $h\nu$ graph. One film's band-gap energy was calculated as 1.52 eV (Fig. 2(b)), which is the ideal value for solar cell applications.

The crystal structure of all samples were determined with x-ray diffraction. Fig. 3 (a) shows the XRD of a CZTS sample. The three sharp peaks at 28°, 47° and 56° are attributed to the (112), (220), and (312) planes of the CZTS respectively. These XRD results show that our sample has a tetragonal crystal structure matching with the JCPDS card no. 26-0575.

We also performed XRD measurements on CZTS samples with different thicknesses (0.15 μm- 11.6 μm). All samples showed the same characteristic peaks. Additionally, we observed that peak intensity increases with thickness (Fig. 3b). FESEM (Fig. 1) and XRD of samples at different thicknesses (Fig. 3b) show that as the thickness increases, the crystallinity and surface quality also increase. The same characteristic peaks and similar increase in crystallinity were observed by various groups in the literature [21,22,24,43].

The crystalline size (D) was calculated through the Debye-Scherrer formula [21, 37],

$$D = \frac{0.9\lambda}{\beta cos\theta}$$

where λ is the x-ray wavelength (0.154059 nm), β is the full-width half maxima which is calculated with the origin software, and θ is the Bragg's diffraction angle. The estimated crystal size of the sample annealed at 150 °C was 24.6 nm, while it was 42.8 nm.

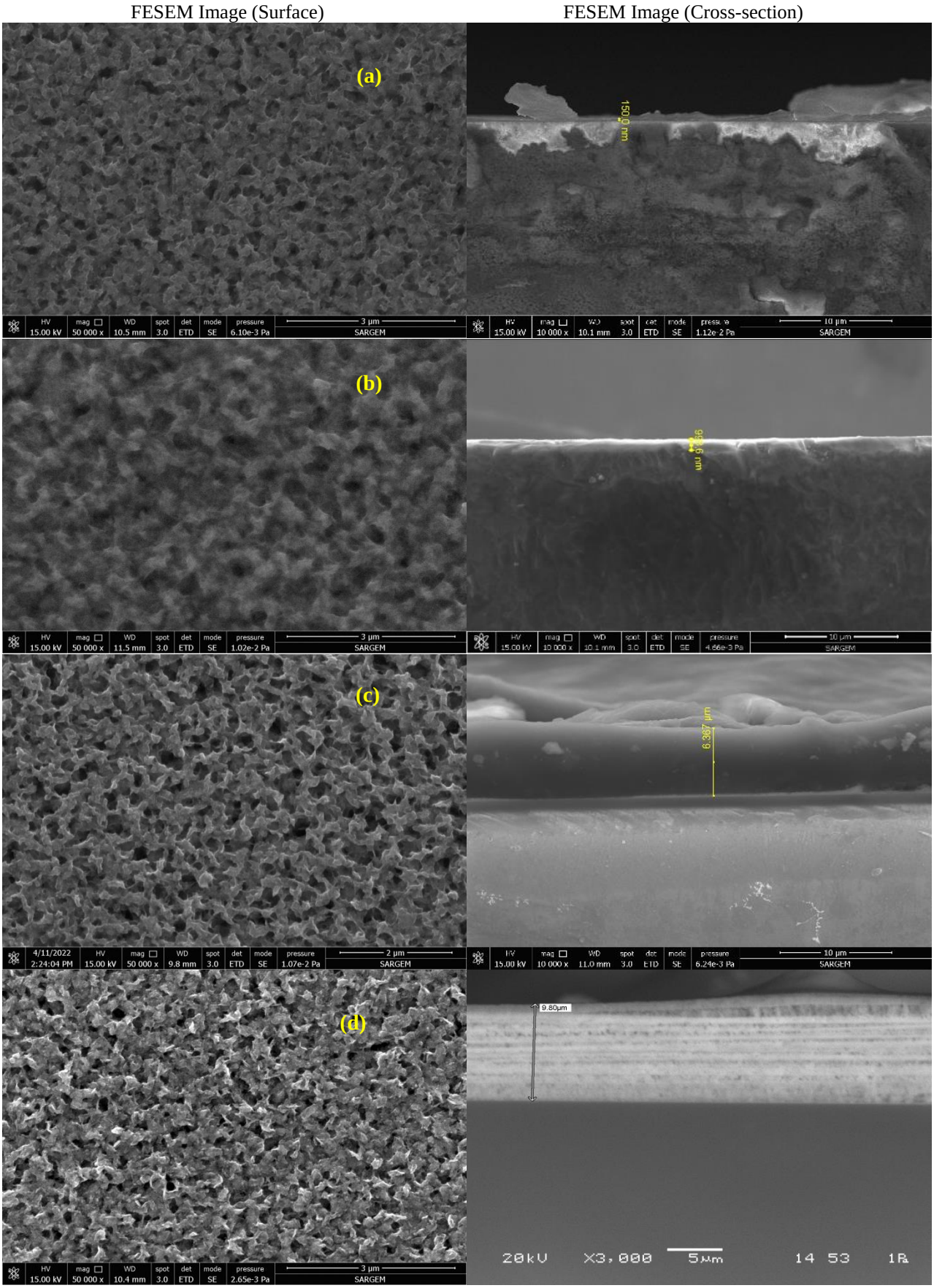

Fig. 1. FESEM and SEM surface and cross-section images of five different samples: (a) 0.15 µm, (b) 0.99 µm, (c) 6.36 µm, (d) 9.80 µm

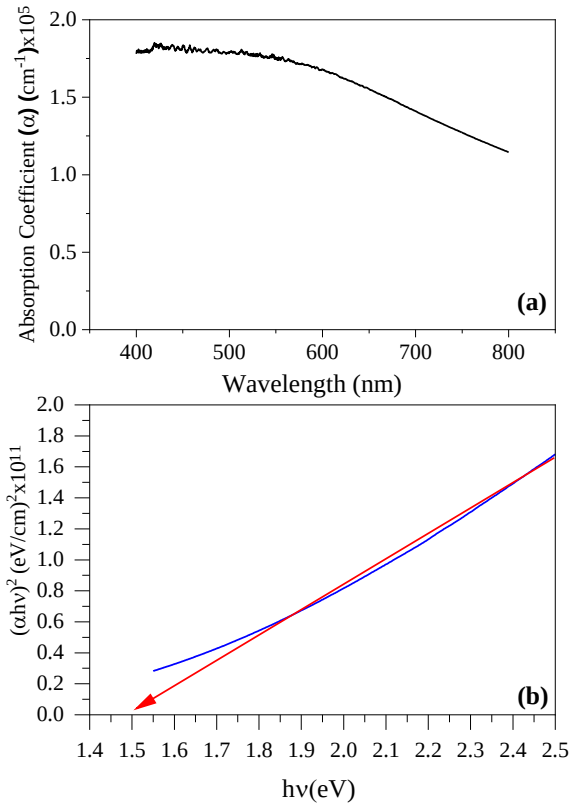

Fig. 2. (a) The UV-visible absorption spectrum of a CZTS thin film, (b) $(h\nu)^2$ vs hν graph of a CZTS sample (color online)

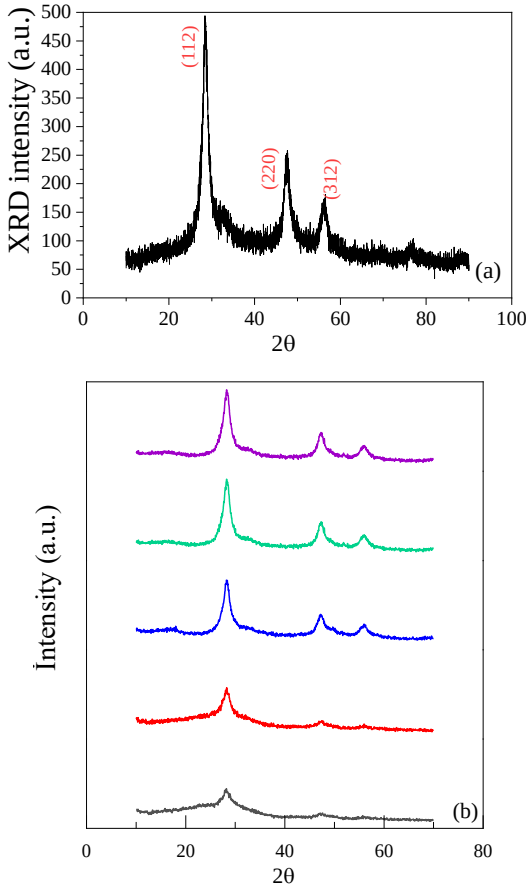

Fig. 3. (a) XRD of a CZTS thin film, (b) XRD responses of CZTS samples with various thickness (0.9-11.6 μm) (color online)

The Raman spectrums of the samples were also taken to prove the formation of the CZTS phase. Fig. 4 shows the Raman spectrum of one such sample.

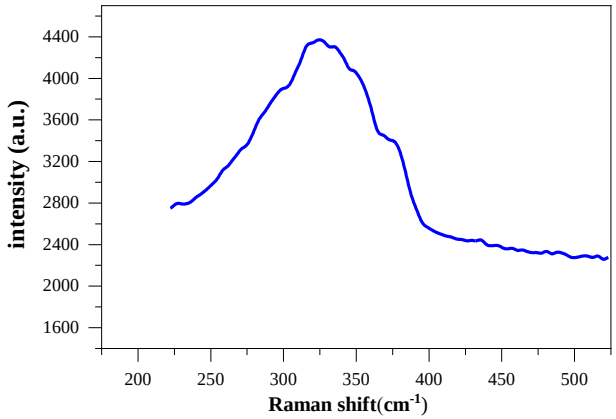

Fig. 4. The Raman spectrum of a CZTS thin film

The Raman spectrum of all samples showed a single Raman intense peak located at 338 cm^{-1}. This value falls within the range of previously reported Raman intense peak values: from 331 cm^{-1} to 338 cm^{-1} [44-48]. The Raman results confirm the XRD results and the fact that the CZTS samples crystallized in the kesterite tetragonal structure.

The effect of annealing on the crystal structure was studied at a lower temperature range (150 °C – 250 °C). To our knowledge, this is the first time the effect of annealing at such low temperatures has been reported. The XRD of the sample before and after annealing is shown in Fig. 5.

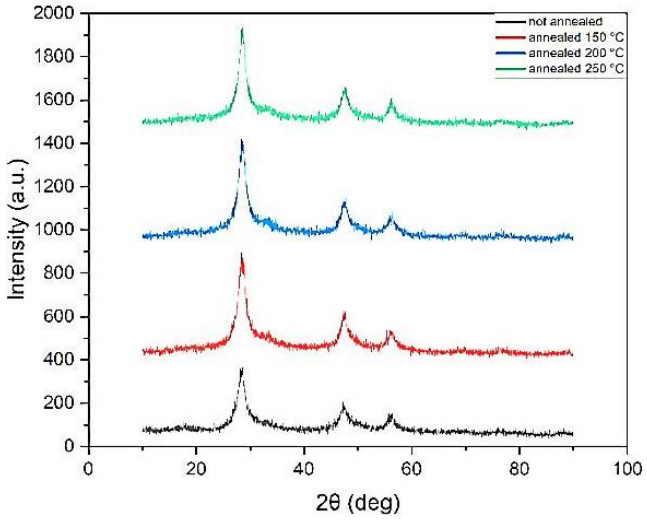

Fig. 5. XRD of the CZTS thin film before and after annealing (color online)

An increase of 30% occured in the XRD peak at 150 °C. At 200 °C this increase was over 30%. After 200 °C,

the increase in XRD response gradually slowed down until 250 °C, where it became stable. It is clear that the peaks at 47° and 56° become sharper as the annealing temperature increases. Two shallow peaks were also observed: one at about 70° and the other at 76°. Sayed et al. observed a similar increase in XRD in annealed CZTS samples [35]. They also observed a peak at 70°, yet their un-annealed samples didn't show a similar result. The increase in XRD at higher annealing temperature may be due to the increase in the crystallite size. As we increased the annealing temperature, we obtained bigger crytallites: the size was 24.6 nm at 150 °C and 42.8 nm at 400 °C. An increase in XRD intensity obtained by annealing has been reported by various groups in the literature [35, 36].

The electrical properties of the CZTS samples were investigated through the Hall effect. Since the Hall effect is dominated by majority carrier transport, our measurements show that CZTS is a p-type material. Table 1 shows our Hall measrement results.

Table 1. The resistivity, mobility, carrier density and conductivity of the CZTS samples

Thickness μm	Volume Resistivity Ω.cm	Mobility $cm^2V^{-1}s^{-1}$	Bulk Carrier Dens. $1\times10^{17}cm^{-3}$	Conductivity $1\times10^2\ \Omega.cm^{-1}$
0.99	16.9	1.33	2.78	7.10
6.36	25.0	1.94	1.28	4.80
9.80	72.1	7.11	0.12	3.14
11.60	65.9	30.5	0.03	2.86

In Table 1, we can see that as the thickness of a CZTS film increases, the mobility and volume resistivity also increase, but the carrier density and conductivity decrease. As the thickness increased from 0.99 μm to 11.6 μm, the mobility increased from 1.33 $cm^2V^{-1}S^{-1}$ to 30.5 $cm^2V^{-1}S^{-1}$. The increase in mobility may be primarily due to the decrease in carrier concentration. Another cause for the increase in mobility may be the decrease in grain boundary scattering. It is reported that as the grain size increases, grain boundary scattering decreases [42]. The increase in volume resistivity may be due to lattice mismatches and impurities that might have occurred between CZTS layers during fabrication. The decrease in carrier density, and thus the conductivity, may be due to the deep-level defects such as Cu_{Zn} [20, 42]. The Cu_{Zn} deep-level defects are predicted to have the lowest formation energy of any defect and provide shallow acceptor states [42, 49]. The increase in the amount of active material may lead to an increase in the number of deep-level defects.

Since the resistivity of the n-type Si substrate is 1×10^{-2} Ωcm, the resistivity obtained in Table 1 should be the resistivity of the CZTS thin films themselves. The effect of Si substrate on the resistivity is negligibly small.

Sarsıcı et al. measured the resistivity of their CZTS as 65 Ωcm and carrier concentration as $10^{15}cm^{-3}$ [57], and Peksu et al. measured resistivity, mobility and carrier concentration of their CZTS samples as 1.2 cm^2/V.s, 16.2 Ω.cm and 3.1×10^{17} cm^{-3} respectively [28]. Also the record IBM device showed the carrier density between 1×10^{15} cm^{-3} and 1×10^{17} cm^{-3} [42]. Our findings are in line with these three reports.

4. Conclusions

In this work, CZTS thin films were coated on a Si substrate by the use of the simple spray pyrolysis technique. CZTS samples at different thicknesses (0.15 – 11.60 μm) were prepared. XRD and Raman spectrum of all films proved that only a CZTS phase was obtained. Electrical measurements showed that increasing the thickness of the film from 0.99 μm to 11.60 μm led to an increase in the mobility of the charged carriers from 1.33 $cm^2V^{-1}S^{-1}$ to 30.5 $cm^2V^{-1}S^{-1}$, as well as that CZTS is a p-type material. Annealing CZTS samples at a relatively lower temperature range of 150-250 °C caused a substantial increase in XRD intensity. An increase of 30% was observed at 150 °C, and an increase of over 30% was recorded at 200 °C. Increasing the thickness of CZTS also contributed to the significant increase in XRD intensity.

This level of increase at such low temperatures may improve the device performance of CZTS solar cells. CZTS solar cells may reach this temperature with concentrated sunlight. Further research needs to be done to prove the effects of annealing on device performance and longevity.

Acknowledgement

We would like to extend our thanks to M. Kaleli and his group for the Hall measurements, and to F. Kayıs and M. Kazanci for the XRD and SEM measurements.

References

[1] J. Mohstasham, Energy Procedia **74**, 1289 (2015).
[2] X. Fontane L. C. Barrio V. İ. Roca, E. Saucedo, A. P. Rodriguez. J. R. Morante, D. M. Berg, P. J. Dale, S. Siebentritt, Appl. Phys. Lett. **98**, 181905 (2011).
[3] G. A. Thopil, C. E. Sachse, J. Lalk, M. S. Thopil, Appl. Energy **275**, 115041 (2020).
[4] A. Blakersa, N. Zina, K. R. McIntoshb, K. Fonga, Energy Procedia **33**, 1 (2013).
[5] P. K. Nayak, S. Mahesh, H. J. Snaith, D. Cahen, Nature Reviews Materials **4**, 269 (2019).
[6] W. Wang, M. T. Winkler, O. Gunawan, T. Gokmen, T. K. Todorov, Y. Zhu, D. B. Mitzi, Adv. Energy Mater. **4**, 1301465 (2014).
[7] A. Polman, M. Knight, E. C. Garnett, B. Ehrler, W. C. Sinke, Science **352**(6238), 4424 (2016).
[8] S. Yuan, X. Wang, Y. Zhao, Q. Chang, Z. Xu, J. Kong, S. Wu, ACS Appl. Energy Mater. **3**(7), 6785 (2020).
[9] R. Kamada, T. Yagioka, S. Adachi, A. Handa, K. F. Tai, T. Kato, H. Sugimoto, IEEE 43rd Photovoltaic Specialists Conference (PVSC) (2016).
[10] M. Nakamura, K. Yamaguchi, Y. Kimoto, Y. Yasaki,

T. Kato, H. Sugimoto, Journal of Photovoltaics **9**(6), 1863 (2019).
[11] M. Aghaei, National Graduate Conference 2012 (NatGrad 2012) Tenaga Nasional Universiti, Malaysia, ISBN 978-967-5770-33-3.
[12] K. Sharma, V. Sharma, S. S. Sharma, Nanoscale Research Letters **13**, 381 (2018).
[13] J. Gong, J. Liang, K. Sumathy, Renewable and Sustainable Energy Reviews **16**, 5848 (2012).
[14] B. S. Arslan, B. Arkan, M. Gezgin, Y. Derin, D. Avcı, A. Tutar, M. Nebioğlu, I. S. Sisman, Journal of Photochemistry & Photobiology, A: Chemistry **404**, 112936 (2021).
[15] J. Y. Kim, J. W. Lee, H. S. Jung, H. Shin, N. G. Park, Chem. Rew. **120**(15), 7867 (2020).
[16] N. S. Kumar, K. C. B. Naidu, Journal of Materiomics **7**(5), 940 (2021).
[17] G. Yılmaz, C. Ozkok, MAKU FEBED ISSN Online:1300-2243 http://dergipark.gov.tr/makufebed
[18] A. Rajagopal, K. Yao, A. K. Y. Jen, Advanced Materials **30**, 1800455 (2018).
[19] D. Yang, X. Zhang, Y. Hou, K. Wang, T. Ye, J. Yoon, C. Wu, M. Sanghadasa, S. (Frank) Liu, S. Priya, Nano Energy **84**, 105934 (2021).
[20] A. S. Nazligul, M. Wang, K. L. Choy, Sustainability **12**, 5138 (2020).
[21] K. Rawat, P. K. Shishodia, Adv. Powder Technol. **28**, 611 (2017).
[22] V. G. Rajeshmon, M. R. R. Menon, C. S. Kartha, K. P. Vijayakumar, J. Analyt. Appl. Pyro. **110**, 448 (2014).
[23] W. Wang, M. T. Winkler, O. Gunawan, T. Gokmen, T. K. Todorov, Y. Zhu, D. B. Mitzi, Adv. Energy Mater. **4**, 1301465 (2014).
[24] K. Diwate, K. Mohite, M. Shinde, S. Rondiya, A. Pawbake, A. Date, H. Pathan, S. Jadkar, Energy Procedia **110**, 180 (2017).
[25] S. Mahjoubi, N. Bitri, M. Abaab, I. Ly, Materials Letters **216** 154 (2018).
[26] K. G. Deepa, T. H. Sajeesh, N. Jampana, Journal of Electronic Materials **47**(1) (2018).
[27] K. G. Deepa, Journal of Analytical and Applied Pyrolisis **117**, 141 (2016).
[28] E. Peksu, M. Terlemezoglu, M. Parlak, H. Karaagac, J. of Crystal Growth **574**, 126336 (2021).
[29] A. Tang, Z. Li, F. Wang, M. Dou, W. Mao, Journal of Material Science: Materials in Electronics **29**(9), (2018).
[30] A. Tang, J. Liu, J. Ji, M. Dou, Z. Li, F. Wang, Appl. Surf. Sci. **383**, 253 (2016).
[31] H. Yang, L. A. Jauragui, G. Zhang, Y. P. Chen, Y. Wu, ACS Nano Letters **12**(2), 540 (2012).
[32] S. D. Sharma, B. Khasimsaheb, Y. Y. Chen, S. Neeleshwar, Ceramics International **45**, 2060 (2019).
[33] X. Xu, Y. Qu, S. Campbell, M. L. Garrec, B. Ford, V. Borrioz, G. Zoppi, N. S. Beattie, Journal of Material Science: Materials in Electronics **30**, 7883 (2019).
[34] H. T. Ali, A. Ashfaq, M. S. Hussain, K. Mahmood, M. Yusuf, S. Ikram, A. Ali, N. Amin, K. Javaid, M. Y. Ali, J. Jakob, M. Anami, Optoelectron. Adv. Mat. **16**(3-4), 164 (2022).
[35] M. H. Sayed, E. V. C. Robert, P. J. Dale, L. Gütay, Thin Solid Films **669**, 436 (2019).
[36] P. Prabeesh, I. P. Selvam, S. N. Potty, Thin Solid Films **606**, 94 (2016).
[37] S. Chamekh, N. Khemiri, M. Kanzari, SN Applied Science **2**, Article number: 1507 (2020).
[38] S. Sanmugavel, M. Srinivasan, K. Aravinth, P. Ramasaway, AIP Conference Proceedings **1942**, 140070 (2018).
[39] Y. Chung, D. Cho, N. Park, K. Lee, J. Kim, Curr. Appl. Phys. **11**, 65 (2011).
[40] J. Han, G. Fu, V. Krishnakumar, C. Liao, J. Wolfram, J. Mater. Sci. Mater. Electron. **77**, 2695 (2013).
[41] İ Candan, Semicond. Sci. Technol. **36**, 115008 (2021).
[42] M. Grosberg, J. Krustok, C. J. Hages, D. M. Bishop, O. Gunawan, R. Scheer, S. M. Lyam, H. Hempel, S. Levcenco, T. Unold, Journal of Physics: Energy **1**, 044002 (2019).
[43] E. M. Mkawi, Y. Al-Hadeethi, E. Shalaan, E. Bekyarova, J. Mater. Sci. **29**, 20476 (2018).
[44] Z. Zakaria, P. Chelvanathan, M. J. Rashid, M. Akhtaruzzaman, M. M. Alam, Z. A. Al-Othman, A. Alamoud, K. Sopian, N. Amin, Jpn. J. Appl. Phys. **54**, 08KC18 (2015).
[45] K Mashood, M. A. Malik, J. Singh, Emergent Materials **4**, 737 (2021).
[46] I. S. Babichuk, M. O. Semenko, R. Caballero, O. I. Datsenko, S. Golovynskyi, R. R. Ziniuk, M. Statsenko, O. A. Kapush, J. Yang, B. K. Li, J. L. Qu, M. Leon, Sol. Energy **205**, 154 (2020).
[47] M. A. Olgar, M. Tomakin, T. Kucukomeroglu, E. Bacaksiz, Mater. Res. Express **6**, 056401 (2019).
[48] K. V. Gunavathy, K. Tamilarasan, C. Rangasami, A. M. S. Arulanantham, Thin Solid Films **697**, 137841 (2020).
[49] H. Ahmoum, P. Chalvanathan, M. S. Suait, M. Bougrara, G. Li, A. H. A. Al-Waeli, K. Sopian, M. Kerouad, N. Amin, Superlattice. Microst. **126**, 32 (2019).
[50] H. M. Shinde, R. J. Deokate, C. D. Lokhande, Journal of Analytical and Applied Pyrolisis **100**, 12 (2013).
[51] M. Ali Olgar, A. Seyhan, A. O. Sarp, R. Zan, J. Mater. Sci: Mater. Electron. **31**, 20620 (2020).
[52] E. Ojeda-Durán, Solar Energy **198**, 696 (2020).
[53] F. Jieng, H. Shen, W. Wang, **41**(8), 2024 (2012).
[54] L. S. Khanzade, M. A. Makhdoom, X. Lin, H. Azimi, C. J. Brabec, Optık **272**, 170381 (2023).
[55] L. Chen, C. Park, Korean J. Chem. Eng. **34**(4), 1187 (2017).
[56] S. Chen, A. Walsh, X. G. Gong, S. H. Wei, Adv. Mater. **25**, 1522 (2013).
[57] S. Sarsıcı, H. K. Kaplan, A. Olkun, R. Mohammadigharehbagh, S. K. Akay, International Journal of Science, Technology and Design **2**(1), 16 (2021).

*Corresponding author: ykarakus@sakarya.edu.tr